

Article

# Thermomechanical Treatment of Martensitic Stainless Steels Sheets and Its Effects on Their Deep Drawability and Resulting Hardness in Press Hardening

Enrique Meza-García <sup>1</sup>, Peter Birnbaum <sup>1,\*</sup>, Pierre Landgraf <sup>2</sup>, Thomas Grund <sup>2</sup>, Thomas Lampke <sup>2</sup> and Verena Kräusel <sup>1</sup>

<sup>1</sup> Institute for Machine Tools and Production Processes, Chemnitz University of Technology, 09126 Chemnitz, Germany; enriquemeza@daad-alumni.de (E.M.-G.); verena.kraeusel@mb.tu-chemnitz.de (V.K.)

<sup>2</sup> Institute of Materials Science and Engineering, Chemnitz University of Technology, 09125 Chemnitz, Germany; pierre.landgraf@mb.tu-chemnitz.de (P.L.); thomas.grund@mb.tu-chemnitz.de (T.G.); thomas.lampke@mb.tu-chemnitz.de (T.L.)

\* Correspondence: peter.birnbaum@mb.tu-chemnitz.de; Tel.: +49-371-5313-3313

Received: 9 October 2020; Accepted: 14 November 2020; Published: 18 November 2020



**Abstract:** The deep drawability of three Martensitic Stainless Steels (MSS) alloys under conventional press hardening thermomechanical process conditions was investigated. The three alloys differ in the content of the main elements C and Cr. Firstly, the metallurgical properties of the alloys were determined, i.e., the phase mass fraction diagrams and the concentration of alloying elements in solid solution at the austenitic temperatures with help of the JMatPro<sup>®</sup> software version 7.0. Derived from this analysis, specific thermomechanical process parameters were defined to evaluate experimentally and numerically the hot sheet formability of the alloys during the deep drawing process. The hot deep drawability of the MSS alloys was experimentally assessed. The hot deep drawability was evaluated with the resulting maximum drawing depth values. In general, all three alloys developed very good formability at forming temperatures between 700 and 900 °C. However, they are susceptible to chemical composition, austenization temperature, dwell time, and flange gap. The hot formability behavior of the alloys as well as the resulting hardness showed very good concordance with the calculated metallurgical values. Finally, a numerical analysis was conducted using Simufact Forming<sup>®</sup> 15.0 software. The interval time during hot blank transfer to the tool determines the initial and final forming temperature. The effect of the time interval on the forming temperature was analyzed numerically and validated experimentally. It was also possible to determine the maximum level of plastic strain in the deep drawn cup.

**Keywords:** thermomechanical treatment; martensitic stainless steel; hot formability; maximum drawing depth; phase transformation temperatures; hardness

## 1. Introduction

Martensitic Stainless Steels (MSS) are Fe-Cr-C alloys with a carbon content between 0.1 and 1 wt %. The content of chromium is typically between 11 and 18 wt % [1]. MSS are characterized by their corrosion resistance combined with high strength. A major advantage of these materials is their high hardness and the resulting high wear and cutting resistance [1]. These materials are currently used, i.e., for cutting tools, turbines, or ball bearings [2]. On one side, bulk formed components made of MSS are usually hot forged. On the other side, the manufacture of sheet metal components is currently carried out by cold forming of the alloys in soft annealed condition. Independently of the forming process, the requested mechanical properties are achieved by a subsequent heat treatment consisting

of quenching followed by tempering. However, for the manufacture of complex sheet components, the degrees of deformation achievable by cold forming are often insufficient. This disadvantage can be counteracted by a combined forming and thermal treatment, i.e., thermomechanical treatment. This basically consists of hot forming of the sheet metal and quenching it simultaneously with the forming tools, which is conventionally better known as the press hardening or hot stamping process. However, until now, only manganese-boron steels are the main alloys used for press hardening. Among these, the 22MnB5 alloy is the most used [3].

The potential of the MSS for the manufacture of sheet metal components by press hardening has already been demonstrated and tested by preliminary investigations and the production of demonstrators [4,5]. In contrast with manganese boron steels, press hardened sheet components made of MSS can achieve ultra-high strengths in combination with very good corrosion resistance. This could enable manufacturing complex lightweight sheet components with longer lifespan, which is highly demanded today. Nevertheless, a basic understanding of the relationships between process parameters, microstructural development, as well as material and service properties such as corrosion is still required [6].

The MSS alloys have been widely characterized mechanically and microstructurally considering conventional bulk forming process conditions [7,8]. However, this information is not enough to evaluate its feasibility to the hot sheet forming processing. The demands on which the blank is formed occur under very different conditions. Firstly, the strains and strain rates developed during sheet forming are substantially lower compared to those developed during bulk forming. Secondly, they will evolve locally, similar to bulk forming but in completely different magnitudes. Their magnitudes will also vary depending on the state of stresses. Thirdly, the magnitudes of the friction coefficients have a considerable influence on formability. All of these features are very difficult to be determined experimentally. Practically, there are not available data about these properties in the literature.

In this work, the hot deep drawability of three selected MSS sheet alloys as well as its relationship to the thermomechanical process parameters was investigated. The aim of this research was to determine the optimal process parameters. Reliable computer aided tools were used for this first approach to analyze the hot sheet formability. They are the Java-based Material Properties (JMatPro<sup>®</sup>, version 7.0, Guildford, UK) and Finite Element Method (FEM)-based Simufact forming<sup>®</sup> software tools (version 15.0, Hamburg, Germany).

In order to undertake a comprehensive analysis, this work has been divided into three sections. The first one deals with a metallurgical analysis of the three different MSS alloys based on thermodynamic calculations performed with the JMatPro<sup>®</sup> Software. In the second section, the hot deep drawability of the alloys was experimentally evaluated. The resulting maximum drawing depth values as a function of the specific process parameters were used to assess the hot formability of the MSS alloys. In the third section, finite elements simulations of the hot deep drawing process evaluated the hot formability of the alloys numerically. The effect of the time interval on the initial forming temperature was analyzed. The level of plastic strains in the deep drawn cup was determined. After a discussion of the results, a summary with the optimal process parameters is included in the conclusions.

## 2. Materials and Methods

### 2.1. Selected Martensitic Stainless Steel Alloys

Three different MSS grades were investigated. These are the X12Cr13, X30Cr13, and X46Cr13 alloys. Table 1 shows the chemical composition of the investigated alloys, which was determined using an optical emission spectrometer Bruker Tasman Q4 (Bruker, Billerica, MA, USA). Carbon was the main alloy element whose content was varied. However, the chromium and manganese contents also increased in line with the carbon content. Table 2 shows the mechanical properties of the MSS alloys in supply conditions (normalized) in rolling direction, which was determined by tensile tests with H&P Inspekt 150 universal testing machine (H&P, Nossen, Germany). All tensile test samples

were 1.5 mm thick, 12.5 mm wide, and 50 mm in gauge length according to DIN EN ISO 6892-1. The impact of anisotropy on mechanical properties was not determined, as its influence is minimal at austenitic temperature.

**Table 1.** Nominal composition of the investigated Martensitic Stainless Steels (MSS) alloys (wt % balance Fe).

Alloy	C	Cr	Si	Mo	Mn	P	S	Ni	Cu
X12Cr13	0.11	11.54	0.50	0.06	0.38	0.021	<0.001	0.33	0.18
X30Cr13	0.35	13.47	0.47	0.94	0.42	0.021	0.001	0.38	0.06
X46Cr13	0.48	13.62	0.47	0.01	0.63	0.026	<0.001	0.17	0.22

**Table 2.** Mechanical properties of the investigated alloys in the as-supplied condition at room temperature in the rolling direction.

Alloy	Condition	Yield Strength (MPa)	Ultimate Tensile Strength (MPa)	Fracture Elongation $A_{50mm}$ (%)
X12Cr13	Normalized	518	651	17
X30Cr13	Normalized	361	611	26
X46Cr13	Normalized	371	633	26

## 2.2. Definition of the Thermomechanical Process Parameters of Relevance

Optimum process parameters should be mainly defined depending on the metallurgical properties of the alloys investigated. However, some specific parameters are defined according to essential technological aspects. Therefore, it is important to establish the ranges of the process parameter of interest that would meet the conventional parameters within the framework of technological feasibility [3]. The most relevant process parameters during hot sheet metal forming are the austenization temperature, dwell time, initial forming temperature, strain rate, tool temperature, and holding time with a closed tool. Table 3 summarizes the range of the process parameters that are of interest in which this research is focused [3].

**Table 3.** Thermomechanical process parameters of interest for this research.

Austenization Temperature ( $T_\gamma$ )/°C	Austenization Time ( $t_{dwell}$ )/s	Initial Forming Temperature $J$ (°C)	Strain Rate/(s <sup>-1</sup> )	Tool Temperature/(°C)	Holding Time with Closed Tools/(s)
950–1150	180–600	700–900	0.1–0.5	20	0, not varied for this research

## 2.3. Metallurgical Analysis Based on Calculations by JMatPro<sup>®</sup> Software

Thermodynamic calculations were employed to predict the phase transformations temperatures in the equilibrium. For this purpose, the software JMatPro<sup>®</sup> 7.0 using Thermotech Fe-database was used. For the calculations, the chemical compositions of the alloys summarized in Table 1 were used. Firstly, the phase mass fraction diagrams of the investigated alloys were calculated to obtain an overview of the phases that are developed in the temperature range of interest described in Table 3. Secondly, the contents of C and Cr alloying elements in solid solution at the austenitic temperatures were estimated.

## 2.4. Experimental Deep Drawing Test

The MSS sheet materials were evaluated using the method of the deep drawing cup test in order to determine the maximum drawing depth. Circular blanks of the alloys with a thickness of 1.5 mm and a diameter ( $D_b$ ) of 170, 180, and 200 mm were austenized and then hot formed into a cup using a drawing punch. The CAD design of the forming tool is illustrated in Figure 1. The tool was mounted into a servo-screw press DUNKES ES1-S4-80/30 (Dunkes, Kirchheim, Germany) with a nominal force

of 800 kN in the ram and 300 kN in the cushion. As a result of the electric drives, very precise motion profiles can be performed and measured by an integrated sensitive positioning system.

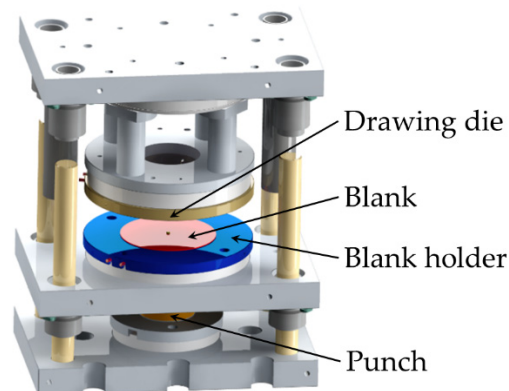


**Figure 1.** CAD design of the deep drawing tool used.

The cylindrical tool used for these experiments produces deep drawn cups with an inner diameter of 100 mm. The drawing gap, i.e., the clearance between the punch sidewall and the ring die, is equal to 2 mm. The drawing ratio  $\beta$  is the relationship between the initial blank diameter  $D_b$  and the punch diameter  $D_{Tool}$  ( $\beta = D_b/D_{Tool}$ ). Thereby, the maximum values of the limiting drawing ratio that could be achieved with this tool set up are 1.7, 1.8, and 2, respectively.

The hot sheet metal forming process is divided in several steps. Initially, the blank is austenized by heating it up to a temperature of 1050 °C or 1150 °C in a furnace. After a dwell time of 300 s, the austenized blanks are transferred into the tool. The temperature of the blank immediately after leaving the furnace was measured by thermocouples, so the time interval needed to cool down the blank to the desired forming temperature was specified accurately. Yet, the forming process takes about 2 s. During this time span, the temperature is not maintained constant, but there are temperature gradients depending on the region of the workpiece. These temperature gradients were precisely determined through the FE simulations, as described in Section 3.3.4. The experimental initial forming temperatures were 700, 800, and 900 °C. The temperature gradient range for experiments conducted at an initial temperature of 700 °C varies exactly between 660 and 750 °C at distinctive points. For experiments performed at an initial forming temperature of 800 °C, this range varies between 680 and 770 °C. Finally, at an initial forming temperature of 900 °C, the range varies between 770 and 890 °C. To facilitate the presentation and discussion of the experimental results, we refer from now on only to the initial forming temperature, i.e., 700, 800 and 900 °C, but we always consider that this is not a constant temperature but a specific range of temperature gradients.

Immediately after the selected forming temperature has been reached, the deep drawing process is started. During this step, the blank is simultaneously formed and quenched by contact with the tool. The MSS sheet materials were evaluated using a ram speed of 20 mm/s with a flange gap (clearance between die and blank holder including the sheet thickness) of 0.5, 1.5, 2.5, and 3.5 mm.

The blank was deep drawn until the fracture of the cup. Then, the maximum drawing depth was determined by using the data of displacement–time and force–time of the press. If a crack occurs during the deep drawing test, load cells of the press will simultaneously register a force drop. Using the collected data of displacement versus time from the press, it is possible to determine the exact position of the tool when the force drop occurs.

Regardless of the flange gap, the maximum allowable drawing depth depends on the blank diameter. For the blank diameter of 170 mm, which corresponds to the smallest one used, the maximum allowable drawing depth is 40 mm. After this depth, there is no more material available between the die and blank holder, and the blank is completely drawn through. Therefore, 40 mm was set up as the maximum drawing depth for all the blank diameters used in order to be able to compare reasonably

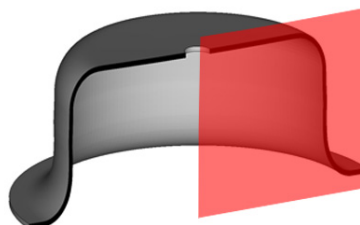
the experimental values. All tests were performed using a boron nitride spray from the company Proline as lubricant.

Table 4 summarizes the experimental parameters used for the deep drawing tests. Due to the broadness of the initial experimental plan, it had to be redesigned in such a way that the results were focused on determining the influence of specific parameters on the maximum drawing depth in a statistically reliable way. In this manner, it was also possible to systematically minimize experimental spending without compromising the statistical quality of the experimental results data. Accordingly, three experiments were performed for each of the conditions selected to guarantee this aspect. The selected parameters were the flange gap, forming temperature, austenization temperature, and drawing ratio. The selected initial austenization temperatures ( $T_\gamma$ ) were 1050 °C and 1150 °C. Two different austenization temperatures were selected, because this parameter has an important effect on the carbide dissolution processes and thus on the chemical composition of the austenite. Moreover, this selection was based on experimental values reported previously [9,10].

**Table 4.** Summarize of the thermomechanical process parameters used for the deep drawing tests.

Austenization Temperature ( $T_\gamma$ ) (°C)	Austenization Time ( $t_{\text{dwell}}$ ) (s)	Initial Forming Temperature (°C)	Blank Diameter (mm)	Flange Gap (mm)	Ram Speed (mm/s)
1050, 1150	120, 300	700, 800, 900	170, 180, 200	0.5, 1.5, 2.5, 3.5	20

After deep drawing trials, cross-sections of the deep drawn cups were cut and mounted on polymer resin for hardness measurements. The resulting Vickers hardness HV1 profile along the sample was measured with an EMCO Test machine (EMCO-TEST, Kuchl, Austria). Figure 2 shows schematically in the red frame the half of the cross-section of the deep drawn cup used for the hardness measurement.



**Figure 2.** Half of the cross-section of the deep drawn cup used for the determination of the resulting hardness.

### 2.5. Deep Drawing Simulation with Finite Element Software Simufact Forming®

Although it is plausible to perform a comprehensive study of the thermomechanical forming process by means of FE simulation with the material database calculated with the JMatPro® software, this first analysis focused mainly on two basic aspects of the process. The first one is the cooling rate of the blank during its transfer from the furnace to the press. This was done in order to compare these results with the experimentally determined cooling rates and thus validate them. The second was the determination of the resulting plastic strain ( $\varphi$ ) in the manufactured cup. This determination is important because  $\varphi$  depends mainly on the tool geometry. Therefore, it will be equivalent in the rest of the alloys investigated.

In future research, the analysis will be extended to the numerical evaluation of the process parameters, the formability limit, as well as the resulting mechanical properties. However, it will first be necessary to determine, validate, and adjust several of the calculated material properties experimentally.

The thermomechanical forming process of the MSS sheet alloys was simulated with Simufact forming® 15.0. The simulation was divided into a handling process of the hot blank in the tool and the subsequent forming process in the press. Prior to the start of the handling process, the blank temperature is set to the austenization temperature. The real time–temperature profile during heating

was not considered in the simulation in order to simplify the process. The handling duration was based on the experimental deep drawing trials. The duration and sequence of the simulated forming process were based on the data of the displacement time of the press for the ram and cushion. The ram speed was kept constant at 20 mm/s until a drawing depth reaches a maximum value of 40 mm. The flange gap (clearance between die and blank holder including sheet thickness) was set to 2.5 mm for all the simulated trials. A simplified CAD model of the deep drawing tool for the FE simulations with the active tool components (punch, blank holder, and die) as well as the workpiece is shown in Figure 3. Tools were modeled as rigid bodies with heat transfer. The blank was modeled in 3D consisting of 31,000 hexahedral elements.

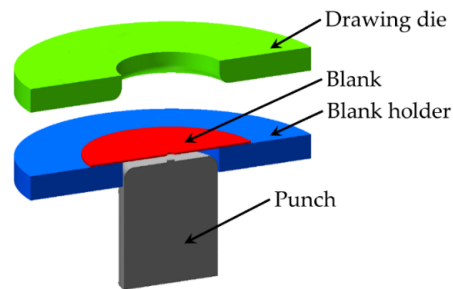


**Figure 3.** Cross-section of the CAD model for Finite Element (FE) simulation.

The material properties of the blank sheet metal alloys required for press hardening simulation were calculated by computer software JMatPro<sup>®</sup> [11] (with general steel database) using the chemical compositions summarized in Table 1. The calculated elastic–plastic material model included flow curves as a function of temperature and strain rate, phase transformation temperatures based on Time Temperature Transformation (TTT) and Continuous Cooling Transformation (CCT) diagrams, as well as physical and thermophysical properties as a function of the temperature. For example, such properties include the density, specific heat, thermal conductivity, thermal expansion coefficient, Young’s modulus, and Poisson’s ratio. A file containing the data of all the material properties was generated and subsequently imported into the material database of the Simufact Forming<sup>®</sup> software. The FE simulations of the press hardening process were carried out separately for each blank alloy material. The plastic strain developed in the component during press hardening was used to characterize the deep drawability of the alloys by FE simulations. In order to properly analyze and compare, specific regions of the resulting component were selected to locally assess the plastic strain. For this purpose, specific points near the surface that are located along the cross-section of the round blank were evaluated. These were separated by a distance of 15 mm from each other, as illustrated in Figure 4. Three points were relevant for the evaluation. Point 1 is close to the center and is located in the bottom of the cup. Point 2 is in the radius region between the bottom and the cup wall. Point 3 is located in the cup wall region close to the cup flange.

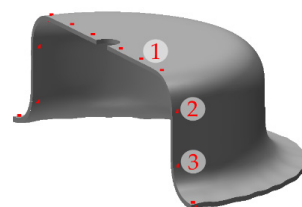


**Figure 4.** Evaluation points in the manufactured cup after the forming process simulation.

### 3. Results

#### 3.1. Metallurgical Analysis

The JMatPro<sup>®</sup> software was used to determine the phases present in the different alloys in the equilibrium state. The results of the thermodynamic calculations indicate a possible formation (or possibly dissolution) of  $M_{23}C_6$ -type precipitates. This must of course be confirmed by a detailed microstructural characterization. For now, the intention of the authors is only to show the possible reasons for the thermomechanical behavior of these alloys. Due to the extensive microstructural analysis, the results will be published in a subsequent publication. The precipitation behavior of MSS as a result of thermomechanical treatments has been investigated in detail before [9,10] and corresponds to the thermodynamic calculations performed. Figure 5a–c show the phase mass fraction in balance as a function of the temperature for the alloys X12Cr13, X30Cr13, and X46Cr13, respectively. In the temperature range of interest, that takes place between 1200 and 600 °C as a result of cooling, all the alloys are transformed from an austenitic phase to a ferritic one and precipitates of the  $M_{23}C_6$  type are developed, too. With the increase of the alloying elements content, the maximum mass fraction of the ferritic phases is reduced from 98% for the X12Cr13 alloy to 91% for the X46Cr13 alloy. In contrast, the maximum mass fraction for the  $M_{23}C_6$  phase increases from 2% for alloy X12Cr13 to 9% for alloy X46Cr13. In the same temperature range but now during heating, it is possible to graphically estimate the temperature at which the alloy will be completely austenized in the equilibrium state. The temperature at which the alloy X12Cr13 reaches an austenite mass fraction >99.98% is  $\approx 905$  °C. With the increasing content of alloying elements, the austenizing temperature rises dramatically to  $\approx 1085$  °C for alloy X30Cr13 and to  $\approx 1125$  °C for alloy X46Cr13. These are at the same time the temperatures required to completely dissolve the possibly present precipitates of the  $M_{23}C_6$  phase.

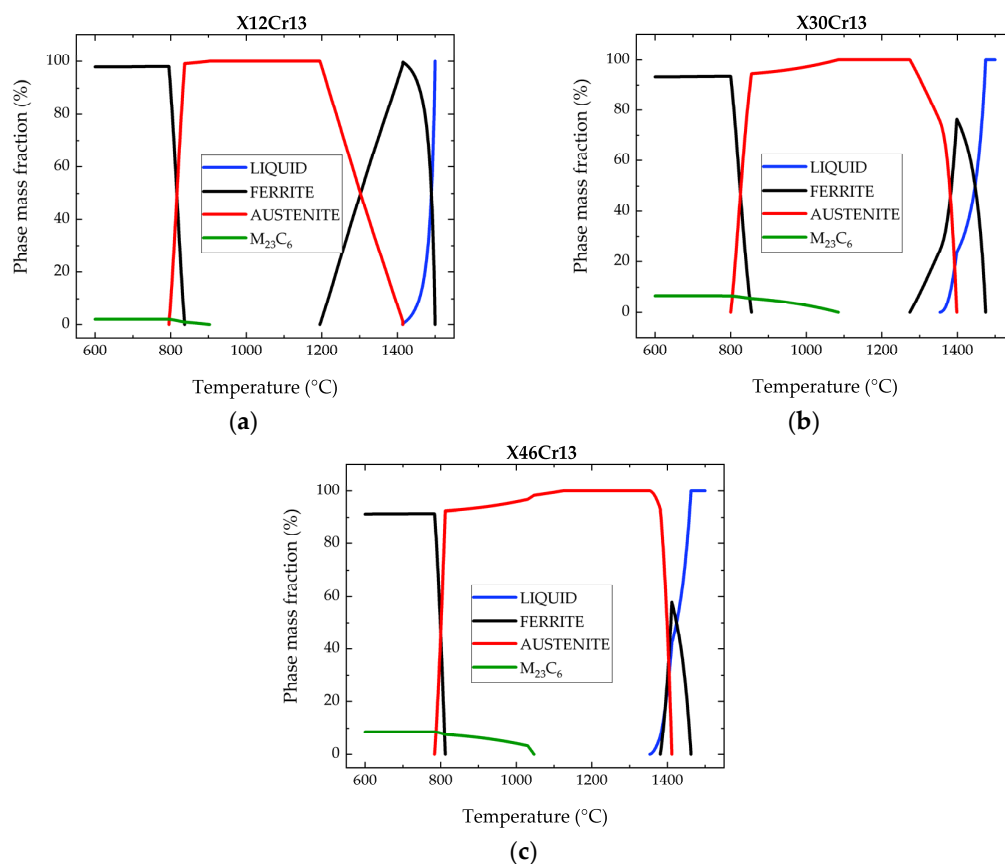


**Figure 5.** Phase mass fraction diagrams as function of the temperature for the X12Cr13 (a), X13Cr13 (b), and X46Cr13 (c) alloys.

As austenization is one of the most important steps during thermomechanical treatment, it is very important to analyze the local chemical composition of the austenite in equilibrium in the austenitic temperature range, that is between 800 and 1200 °C. Figure 6a–c show the mass fraction of main alloy elements, i.e., C and Cr dissolved in austenite for all the investigated alloys. For the X12Cr13 alloy, it is possible to achieve the maximum solubility of C and Cr at temperatures of 905 °C, respectively. For the X30Cr13 alloy, the maximum solubility of C and Cr is achieved at 1085 °C and for the X46Cr13 alloy, it is achieved at 1125 °C. Namely, the temperature at which maximum solubility is reached rises with increasing alloy element content.

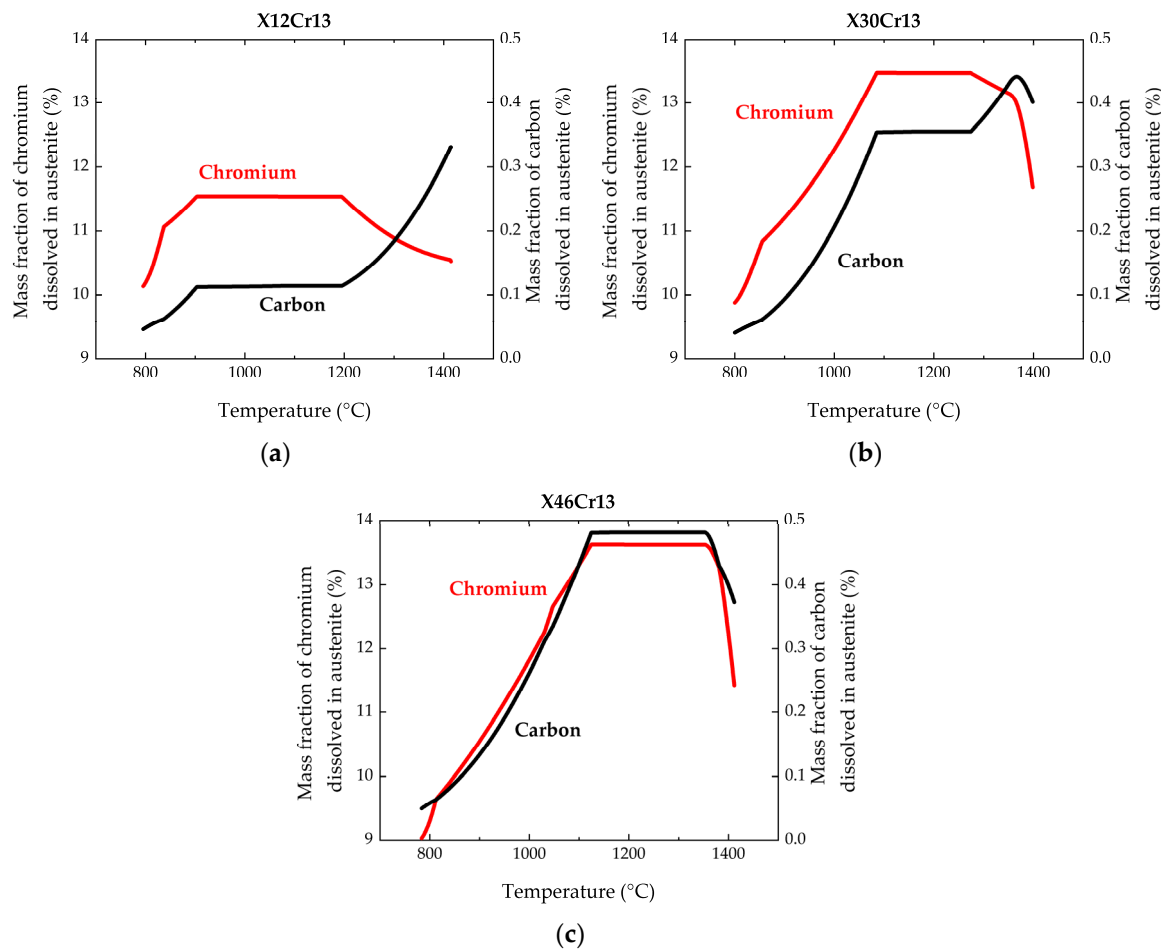


**Figure 6.** Mass fraction of the contents of C and Cr alloying elements in solid solution at the austenitic temperatures, i.e., between 800 and 1400 °C for the X12Cr13 (a), X13Cr13 (b), and X46Cr13 (c) alloys.

### 3.2. Hot Deep Drawability of the MSS

#### 3.2.1. Influence of the Flange Gap and Initial Forming Temperature on Maximum Drawing Depth

To perform this analysis, experimental trials were selected where three parameters are kept constant. These are an austenization temperature ( $T_\gamma$ ) of 1050 °C, a dwell time ( $t_{\text{dwell}}$ ) of 300 s, and a blank diameter of 170 mm. The determined maximum drawing depth values are summarized in Figure 7a–c for the different MSS alloys.

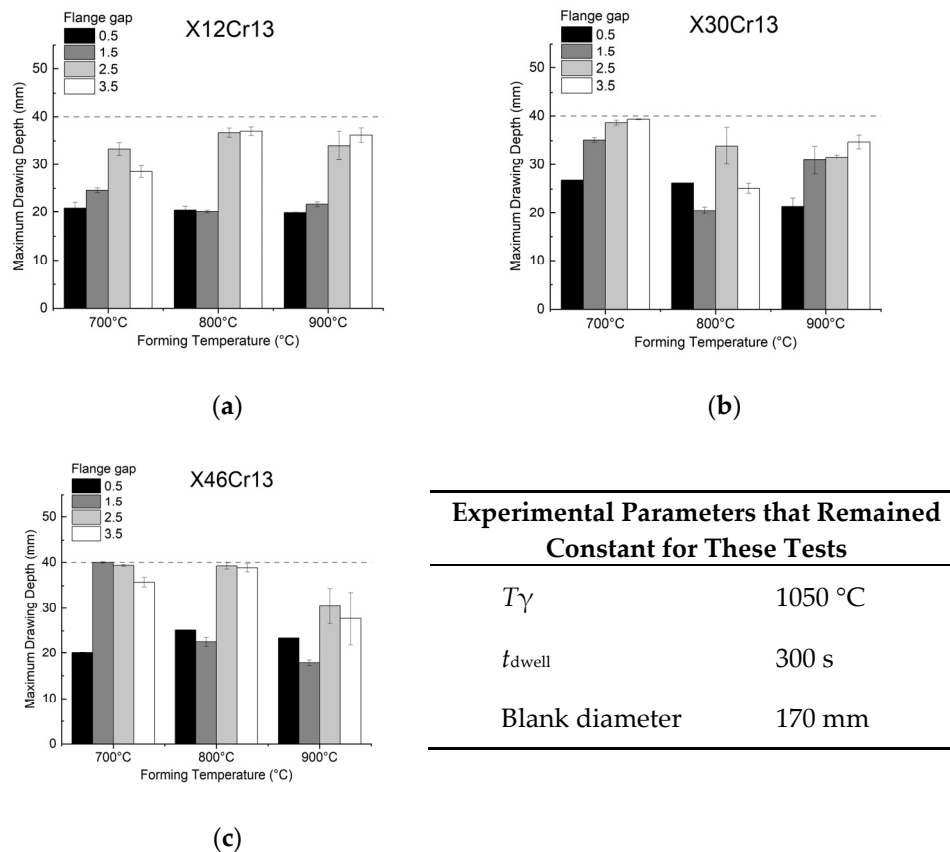


**Figure 7.** Maximum drawing depth as function of the flange gap and initial forming temperature for the X12Cr13 (a), X30Cr13 (b), and X46Cr13 (c) alloys.

In general, with the increase of the flange gap, there was an increase in the maximum drawing depth of the deep drawn cups. On average, the best results were obtained with flange gaps of 2.5 and 3.5 mm. Under these conditions, the X30Cr13 and X46Cr13 alloys could reach the limit of 40 mm, as shown in Figure 7b,c. The effect of temperature on deep drawability was more dependent on alloy composition. In the case of the X12Cr13 alloy with the lowest alloying element contents, the maximum drawing depth values increased with the increase of temperature. However, temperature had the opposite effect with the progressive increase in alloying element content. The high alloyed X30Cr13 and X46Cr13 steels achieved their maximum drawing depth at an initial forming temperature of 700 °C, which was the lowest initial forming temperature, as shown in Figure 7b,c. The values obtained at higher temperatures are not at all negative, but they contrast considerably because the formability of these alloys reached the limit of 40 mm.

### 3.2.2. Influence of the Austenization Temperature and Initial Forming Temperature on Maximum Drawing Depth

To perform this analysis, experimental trials were selected where two parameters are kept constant. These are a blank diameter of 170 mm and a flange gap of 2.5 mm. The increase of the austenization temperature from 1050 to 1150 °C had in general a positive impact on the deep drawability for all the MSS alloys, as shown in Figure 8a–c. Similarly, the increase in dwell time from 120 to 300 s at 1150 °C had a positive impact, too. For a combination of the highest austenization temperature at 1150 °C with the longest dwell time of 300 s, it was possible to manufacture crack-free cups until the limit of 40 mm for all the MSS alloys at all tested forming temperatures. It is also noteworthy that in the case of the other austenization temperatures, the formability of the X30Cr13 and X46Cr13 alloys tends to decrease slightly when the initial forming temperature increases to about 900 °C.

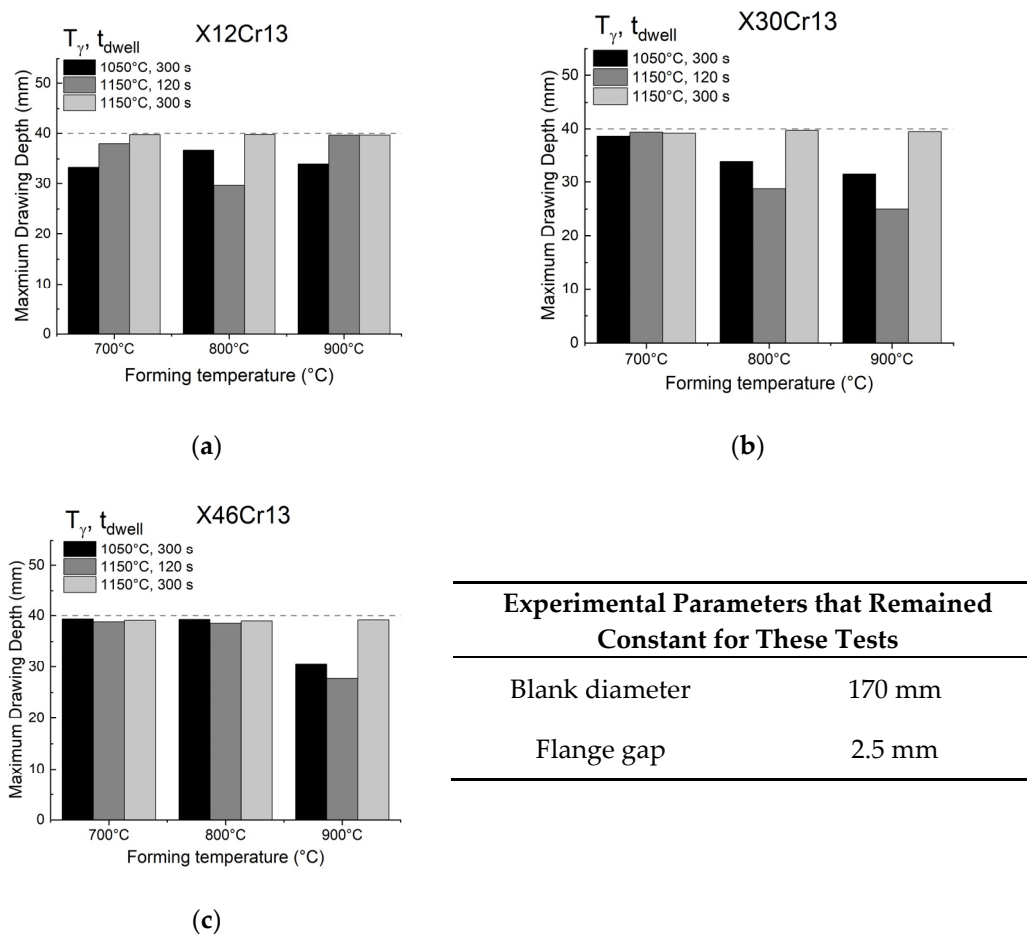
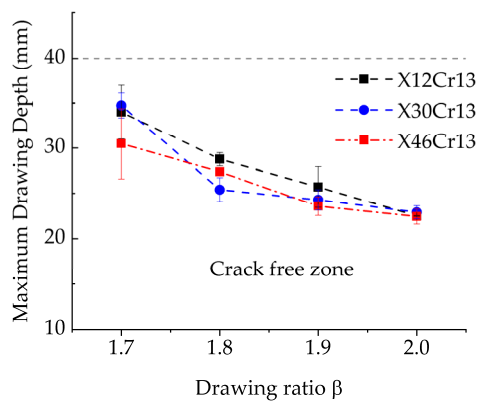


**Figure 8.** Maximum drawing depth as a function of the austenization temperature and initial forming temperature for the X12Cr13 (a), X30Cr13 (b), and X46Cr13 (c) alloys.

### 3.2.3. Influence of the Drawing Ratio on Maximum Drawing Depth

To perform this analysis, experimental trials were selected where four parameters were kept constant: an austenization temperature of 1050 °C, a dwell time of 300 s, an initial forming temperature of 900 °C, and a flange gap of 2.5 mm.

Figure 9 summarizes the maximum drawing depth as a function of the drawing ratio for all the investigated MSS alloys, which is practically the limit up to which the material can be deformed without cracking. In order to delineate better this limit in the diagram, the dots have been joined by means of a line indicating the trend linearly. In general, the maximum drawing depth tends to decrease with the increase of  $\beta$  or blank diameter. At least under these testing parameters, the determined maximum drawing depth trends do not vary significantly between different alloys. The minimum drawing depth value was of 22.5 mm for a  $\beta$  value of 2 and the maximum drawing depth was between 30 and 35 mm for a  $\beta$  value of 1.7 for all the alloys. Only the X12Cr13 alloy showed a slightly better formability in comparison to other alloys under these conditions. Considering the previous results, it is possible to establish that the drawing depth values of the MSS alloys can be improved significantly (until the limit of 40 mm for  $\beta = 1.7$ ), if the austenization temperature or the flange gap is increased and if an adequate deformation temperature is selected according to the alloy, as shown in Figures 7 and 8.



Experimental Parameters that Remained Constant for These Tests	
$T_{\gamma}$	1050 °C
$t_{dwell}$	300 s
Initial forming temperature	900 °C
Flange gap	2.5 mm

Figure 9. Maximum drawing depth as a function of the drawing ratio.

### 3.2.4. Hardness Profile of the Deep Drawn Cups

The resulting Vickers hardness (HV) profiles of the deep drawn cups are shown in Figure 10. For this analysis, experimental trials were selected where two parameters are kept constant. All the samples corresponding to the experiments were performed with a blank diameter of 170 mm and a flange gap of 2.5 mm. The upper of the sample corresponds to the cup bottom, the vertical part corresponds to the cup wall, and the lower part corresponds to the flange cup.

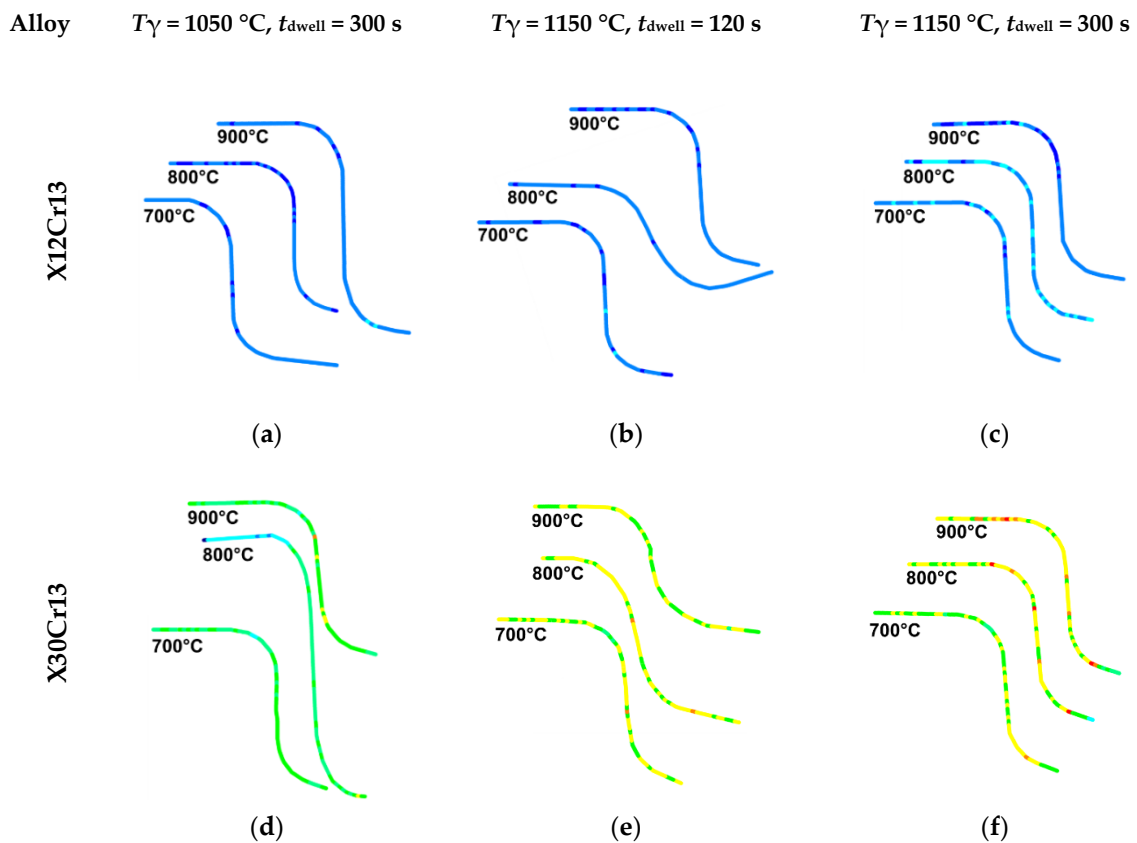
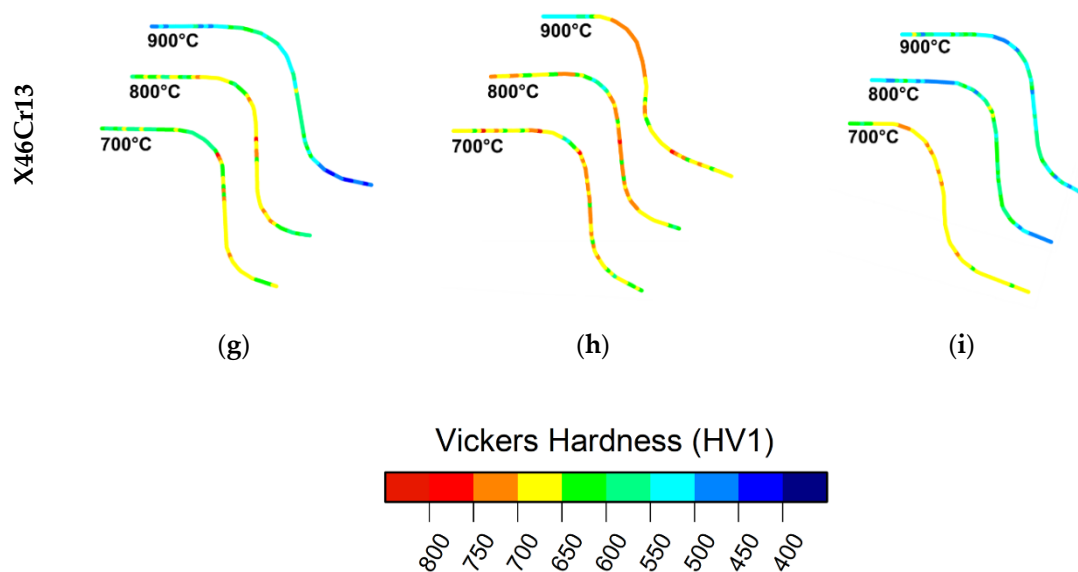


Figure 10. Cont.



**Figure 10.** Resulting Vickers hardness profile of the deep drawn cups of the MSS alloys as a function of the austenization temperature  $T_\gamma$  and dwell time  $t_{\text{dwell}}$  for X12Cr13 (a–c), X30Cr13 (d–f) and X46Cr13 (g–i) depending from the austenitization treatment.

The most influential factor in the resulting hardness was definitely the chemical composition, i.e., the alloying element contents. As expected, the higher the C, Mn, and Cr content, the higher the resulting hardness. The lowest hardness values correspond to the deep drawn cups of the X12Cr13 alloy with values between 400 and 500 HV1, whereas the highest hardness values resulted from the cups made of the X46Cr13 alloy with values between 550 and 750 HV1.

As clearly shown in Figure 10, the austenization temperature and dwell time also have a significant effect on the resulting hardness. With increasing austenization temperature and dwell time, the resulting hardness values of the X12Cr13 and X30Cr13 alloys also increased. However, in the case of the X46Cr13 alloy, the highest hardness values correspond to those of the austenized blanks at a temperature of 1150 °C but for a shorter dwell time of 120 s. When the dwell time interval increases to 300 s, the hardness values decreased slightly. This is most likely due to the increase in dwell time to 300 s, which according to Figure 6 causes the chemical composition to approach equilibrium. That is, a greater amount of potential precipitates of the type  $M_{23}C_6$  dissolve, and thus, the concentration of carbon in solid solution increases. As a result, a greater fraction of retained austenite will be developed after quenching, and thus, the hardness decreases.

In the case of the initial forming temperature, when it increases, the resulting hardness values also tend to increase slightly in the cups of the X12Cr13 and X30Cr13 alloys. Only in the case of the X46Cr13 alloy does it tend to increase slightly when the initial forming temperature decreased progressively until 700 °C.

### 3.3. FE Simulation of the Deep Drawing Process

The simulative modeling of the experimental forming process allows estimating the occurring plastic deformation and in which temperature range this deformation occurs depends on the position in the workpiece. The simulation model corresponds in its geometry to the active parts of the forming tool and in its material properties to the investigated alloys. The simulation was performed exclusively for forming processes after an initial austenitizing temperature of 1050 °C.

#### 3.3.1. Validation of the Cooling Rates Numerically Simulated with the Experimental

The cooling rates of the round blanks after austenization were determined experimentally in order to compare them with those obtained numerically. This was useful to validate the results

obtained in the FE simulation. For this aim, a thermocouple was spot-welded to the round blank surface exactly over the point 1 position, and thus, the temperature could be measured as a function of time. The initial austenitization temperature for this evaluation was 1050 °C for all the alloys. Figure 11 shows an exemplary comparison of the experimental and numerically simulated cooling curves of the X12Cr13 alloy with Heat Transfer Coefficient (HTC) = 10 W/(m<sup>2</sup> K) and emissivity  $\epsilon = 0.6$ . In general, the simulated cooling (time–temperature) curves were comparable for all investigated alloys. Therefore, the thermal properties in the austenitic region were only marginally affected by the chemical composition of the alloys. It is obvious that the experimental and simulated curves completely overlap, exactly identical to the other two alloys. Figure 11 shows the cooling sequence until the blank reaches a temperature of 950 °C. Therefore, it completely covers the primary cooling phase immediately after the austenitized blank leaves the furnace.

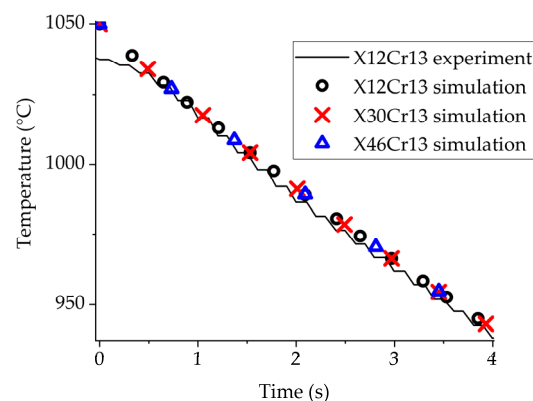


**Figure 11.** Comparison of the experimental and numerical simulated cooling curves of the X12Cr13 alloy from an austenitization temperature of 1050 °C. Simulated cooling curves of the X30Cr13 and X46Cr13 alloys are also shown in the comparison.

### 3.3.2. Contours Levels of the Plastic Strain

The level of plastic strain ( $\phi$ ) that develops during the forming process depends essentially on the forming tool geometry. In this research, the forming tool design did not change. Consequently, the level of plastic strain developed will be the same regardless of the chemical composition of the evaluated alloys. As an example, Figure 12 shows the contour of the plastic strain levels developed in the cup resulting from the deep drawing process on the X12Cr13 alloy. The friction coefficient according to Coulomb is constant at  $\mu = 0.2$ . The heat transfer coefficient to the environment is temperature-dependent, and the heat transfer coefficient between the tool and workpiece is dependent on the contact pressure.

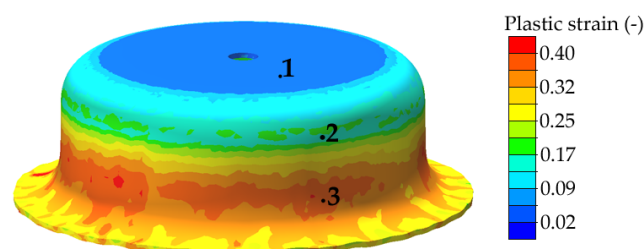


**Figure 12.** Contour levels of the plastic strain after the forming process for the X12Cr13 alloy after austenitization at 1050 °C and 900 °C initial forming temperatures.

As can be seen in Figure 12, the lowest level of plastic strain occurred in the cup bottom region (Point 1 or punch region). Here, the level of plastic strain increased only slightly below a value of  $\phi = 0.1$ . In the radius region (Point 2 region) between the bottom and the cup wall, the plastic strain increased

to a value of  $\varphi = 0.2$ . Progressively, the region with the highest level of plastic strain, i.e.,  $\varphi = 0.4$ , was the one located between the cup wall and the flange (Point 3 region). Wrinkle development is evident in the flange region. There, the level of  $\varphi$  varied between 0.25 and 0.35.

### 3.3.3. Interaction between Plastic Strain and Cooling Rate

Figure 13 shows the local interaction between  $\varphi$  and forming temperature at points 1, 2 and 3 of the cup for the X12Cr13 alloy. The time–temperature sequences cover the process period from transfer of the heated blank to the tool to completion of the forming step. As expected, the cooling rate in the region of point 1 was kept constant until the end of the forming process. In addition, the lowest  $\varphi$  value of less than 0.05 was achieved in this region.

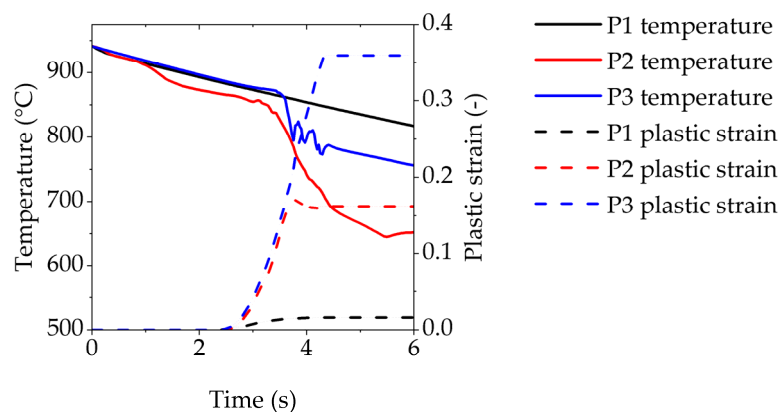


**Figure 13.** Local interaction between plastic strain and workpiece temperature at points 1, 2 and 3 of the cup for the X12Cr13 alloy from FE simulation after austenitization at 1050 °C and immediate transfer.

In the region of the point 2, it can be seen that the cooling rate remains constant only at the beginning of the process but increases sharply during the forming process. This occurred because in this region, the blank metal came into contact with the active tools components and remained in contact until the completion of the forming process. As a result, this region is characterized by the highest cooling rate of around about 55 °C/s.

In order to illustrate in more detail what occurs in this region, Figure 14 shows the developed contact pressure in the workpiece. As clearly indicated by the contour levels of the pressure contact, the highest level is reached along this region. Pressure contact values in this region are ranging between 90 and 135 MPa. This is because the region of point 2 is located precisely in the region of the punch radius. During the forming process, the drawing forces are concentrated predominantly along the entire circumference of the punch radius. This is the reason why the cooling rate is strongly accelerated in this region.

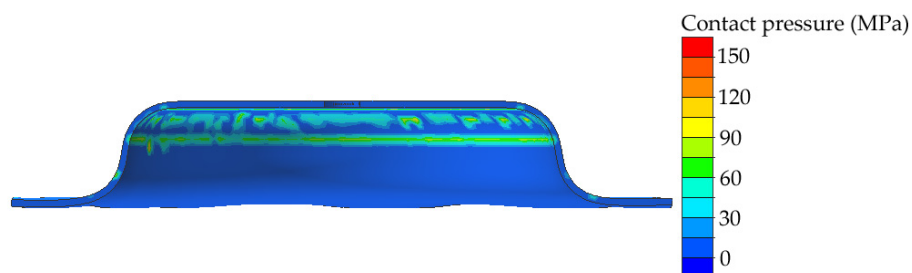


**Figure 14.** Contour levels of the developed contact pressure during workpiece forming for the X12Cr13 alloy simulated numerically (cross-sectional view).

In contrast to the point 2 region, the region of point 3 is characterized by the highest level of  $\varphi$ , reaching a value of 0.4. Nevertheless, the cooling rates are not as high as in the point 2 region, as clearly shown in Figure 13 (see blue line). The reason for this is that the contact pressures in this region are significantly lower than those in the punch radius region, as indicated in Figure 14.

Regardless of the region, the forming step begins once about 2.5 s have elapsed during the transfer of the blank to the press and the closing of the press, as shown in Figure 13. Right at this time, the blank temperatures are in the range of 870 to 890 °C from former 1050 °C. The forming stage ends after 4.3 s, and at this time, the workpiece temperature is between 700 and 850 °C ( $\Delta T = 150$  °C).

### 3.3.4. Effect of the Time Interval during Blank Transfer on the Initial Forming Temperature

Analogous to the experimental trials, the desired initial forming temperature was reached after allowing the austenitized blank to cool down for a specific time interval. This process step was also transferred to the simulation to analyze the effect it has on the initial forming temperature as well as on the workpiece temperature during the forming process.

Figure 15 shows the motion profile of the blank holder and drawing die in the press while forming including different initial time intervals after austenitization and transfer. These time intervals were: case (a) immediate transfer (see Figure 15a), case (b) after 3 s (see Figure 15b), and case (c) after 8 s (see Figure 15c). Thus, the initial forming temperature was different for each of the intervals, exactly as it happened during experimental trials.

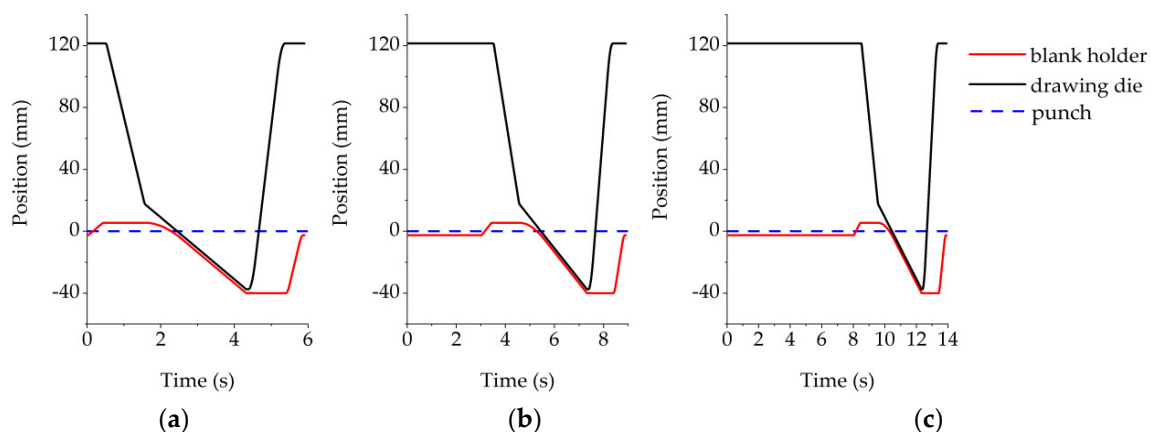


**Figure 15.** Motion profile of blank holder and drawing die in the press while forming in comparison to the constant top level of the punch at 0 mm (reference height) for different soaking time intervals: case (a) immediate transfer, case (b) after 3 s, and case (c) after 8 s.

Before the forming process starts, the blank is positioned exactly as shown in Figure 1. Apparently, the sheet contacts the blank holder (in blue color), although this is not the case. The punch is located a couple of millimeters above the horizontal level of the blank holder; thus, when the hot blank is placed on the tool, only the central part (point 1 region) is in direct contact with the top surface of the punch. Hence, contact of the critical workpiece regions (point 2 and 3) with the blank holder is avoided, and cooling will only depend on contact with the ambient air. When starting the forming operation, the blank holder lifts the workpiece above the punch to obtain a synchronized motion between forming the die and blank holder before touching the punch. So, the regions of point 2 and 3 will be clamped between drawing the die and blank holder during synchronization, which leads to a higher cooling rate. When forming takes place, the high contact pressure at the drawing edges of the die and the punch will increase the cooling rate additionally, whereas the region at point 1 just exhibits minor cooling due to a lowered contact pressure to the punch surface.

Figure 16 shows the cooling curves and the plastic strain for the X46Cr13 alloy after austenitization at 1050 °C and transfers in the three different regions (points 1, 2, and 3, see Figure 12) including different initial time intervals analog to Figure 15.

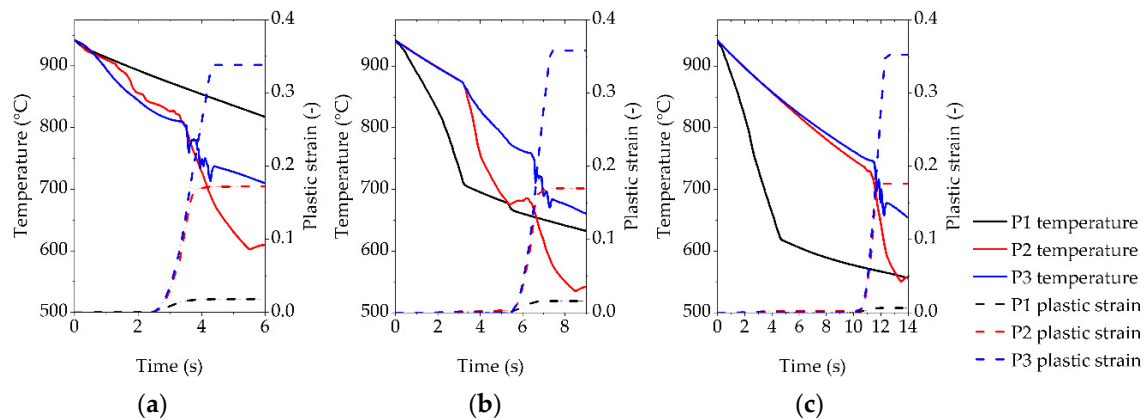


**Figure 16.** Temperature–plastic strain vs. time diagram for the X46Cr13 alloy during blank transfer and forming step from an initial austenitization temperature of 1050 °C for different soaking time intervals: case (a) immediate transfer, case (b) after 3 s, and case (c) after 8 s.

If we compare the diagrams for X46Cr13 in Figure 16, it is obvious that longer time intervals lead to lower initial forming temperatures. In case (a), when forming begins immediately after transfer (see Figure 16a), the initial forming temperatures in the regions of points 2 and 3 are between 820 and 840 °C. Consequently, the temperatures at the end of the forming process decrease to values between 680 and 730 °C for points 2 and 3, respectively. The temperature in points 2 and 3 drops more rapidly in comparison to point 1 because at the beginning, the blank holder lifts the workpiece in that contact area for synchronization, whereas in point 1, the sheet is not in contact with the punch anymore.

In case (b), after a time interval of 3 s (see Figure 16b), the initial forming temperatures are between 680 and 770 °C for points 2 and 3, respectively. Point 1 has now the highest cooling rate because the workpiece remains longer (3 s) on the punch. Subsequently, the temperatures at the end of the forming process in the same regions are between 570 and 680 °C. In the region of point 2, which is the most thermally influenced region, the temperature at the end of the process dropped to below 600 °C.

In case (c), after a time interval of 8 s (see Figure 16c), the initial temperature achieves at point 2 and 3 values between 730 and 750 °C which drops to temperatures between 600 and 670 °C at the end of the forming process. In this case, the temperature ranges are comparable to those of case (b). Again, point 1 exhibits higher cooling rates at the beginning, because this region remains for 8 s on the punch.

In summary, the initial forming temperatures for all three regions after blank austenitization at 1050 °C and followed by rapid transfer will be between 820 and 880 °C. If the time intervals during the transfer are extended to 3 or 8 s, the initial forming temperatures will decrease to values between 570 and 750 °C, respectively. Regardless of this temperature variation, it is assumed that the alloys will remain in their austenitic state. Nevertheless, Continuous Cooling Transformation (CCT) has to be experimentally determined to confirm this. Special attention should point to the effect of a cooling rate of about 55 °C/s on the phase transitions, since this is the value achieved in the most sensitive region of the workpiece (point 2).

## 4. Discussion

### 4.1. Phase Transformation Temperatures

According to Figure 5, the selected austenizing temperatures are well above the ferrite to austenite transformation temperature. However, as also indicated in Figure 6, the increased contents of the alloying elements also promote the formation of  $M_{23}C_6$ -type precipitates and delay their complete

dissolution in the austenitic matrix, which is assumed with the help of thermodynamic calculations. Therefore, complete austenitization of all alloys cannot be guaranteed. Therefore, it is necessary to establish a correlation between formability and microstructure, i.e., the determination of the main alloying element content in the austenitic phase and grain size as well as the chemical composition of precipitates potentially present in the alloys. For this purpose, it is necessary to characterize the input and cup materials manufactured microstructurally. Although it is beyond the scope of this research, this characterization research will be performed in the future. In particular, it is very important to evaluate the impact of thermomechanical treatment on corrosion resistance.

#### 4.2. Influence of the Process Parameters on the Hot Deep Drawability

##### 4.2.1. Influence of the Flange Gap and Initial Forming Temperature on Maximum Drawing Depth

The implementation of the larger flange gaps of 2.5 and 3.5 mm had a very positive impact on the hot deep drawability of all investigated alloys. These results are in good agreement with previous experimental results [12–14]. Although the austenitization temperature was the lowest (1050 °C), it was possible to manufacture crack-free cups until the maximum drawing depth limit of 40 mm with the highly alloyed steels (i.e., X30Cr13 and X46Cr13 alloys). Moreover, the optimum formability performance of these alloys was achieved in combination with the lowest initial forming temperature of 700 °C, which seems at first sight contradictory. However, previous research with the X46Cr13 alloy showed that tensile tests performed at temperatures between 600 and 1000 °C developed a similar behavior [14]. The ductility of this alloy reached its maximum at temperatures between 700 and 800 °C and then decreased at higher temperatures. Namely, the elongation at fracture was 72% at 800 °C, while at 1000 °C, it was 46%. Of course, this phenomenon should be correlated to microstructural changes that develop in this temperature range. In particular, the content of alloying elements in solid solution, the dissolution or formation of precipitates, as well as the interaction of these changes on grain growth kinetics and recrystallization are worth examining.

##### 4.2.2. Influence of the Austenization Temperature and Forming Temperature on Maximum Drawing Depth

The increase of the austenization temperature from 1050 to 1150 °C as well as the increase in dwell time from 120 to 300 s at 1150 °C had in general a positive impact on the deep drawability for all the MSS alloys. Consequently, the optimum combination was an initial austenization temperature at 1150 °C with a dwell time of 300 s. Under these conditions, it was possible to manufacture crack-free cups until the maximum drawing depth limit of 40 mm for all the investigated MSS alloys under all tested forming temperatures. As shown in Figure 6, with increasing austenizing temperature, the amount of  $M_{23}C_6$ -type precipitates will be reduced, and a higher content of alloying elements such as C and Cr will be present in solid solution. Thus, the austenitic matrix will have less impurities or obstacles for the dislocations slip. Therefore, formability will improve under these conditions.

Once again, as in the case previously discussed, the highly alloyed MSS developed a slight detriment to their formability with increasing forming temperature. Although not dramatic, it correlates well with previous results.

It is important to mention that in general, the maximum drawing depth values achieved by these alloys are quite significant. Just to compare, the conventional press hardening alloy 22MnB5 reached a value of 25 mm using the same tool geometry and very similar process parameters [12]. Thus, it should be emphasized that the high ductility of these alloys is quite remarkable.

##### 4.2.3. Influence of the Drawing Ratio on Maximum Drawing Depth

In cold sheet forming processes, it is possible to close the blank holder and die tools to hold the blank and thus set up a blank holder force. In this way, it is possible to determine the boundaries between the formation of wrinkles and the formation of cracks, i.e., the process window. In hot sheet metal forming processes, it is not possible to apply this method, because it is always necessary to

set up a flange gap [3,12,13]. However, through the relationship between the drawing ratio and the maximum drawing depth shown in Figure 9, it is possible to outline a limit up to which the material can be plastically deformed without cracking, at least under the indicated parameter processes that are kept constant.

If the remaining experimental results that are not included in Figure 9 were considered, it would be clear that the limit could be considerably extended if certain parameters vary. More precisely, the maximum drawing depth value can achieve a value of 40 mm, at least by using blanks with a diameter of 170 mm ( $\beta = 1.7$ ), if the austenization temperature or the flange gap is increased and if an adequate deformation temperature is selected according to the alloy, as demonstrated in Figures 7 and 8. Therefore, this method could be a suitable alternative to determine the limits of fracture formation during press hardening.

#### 4.2.4. Hardness Profile of the Deep Drawn Cups

Noteworthy for the resulting hardness was its variation depending on the chemical composition and the initial forming temperature. On the one hand, the hardness values of the alloys X12Cr13 and X30Cr13 increased progressively with the increase of the austenization temperature and the dwell time, in which  $T_{\gamma} = 1150$  °C and  $t_{\text{dwell}} = 300$  s are the optimal values to reach the maximum hardness. The initial forming temperature had no significant effect on the hardness of these particular alloys.

On the other hand, the highest hardness of the highly alloyed steel X46Cr13 was also achieved at  $T_{\gamma} = 1150$  °C but with a shorter  $t_{\text{dwell}} = 120$  s. Furthermore, it is very noticeable in Figure 10g–i that for this alloy, the initial forming temperature has a significant impact on the hardness. As the initial forming temperature decreases, the hardenability of the steel also improves, reaching its highest values at an initial forming temperature of 700 °C. Then, as discussed previously, the effect of the initial forming temperature is consistent with the effect on the hot drawability, i.e., the maximum drawing depth. Consequently, it has to be correlated with the microstructural development.

#### 4.3. Plastic Strain and Workpiece Temperature Sensitivity

By means of the numerical simulation of the deep drawing process, it was possible to determine that the workpiece region with the highest level of plastic strain, i.e.,  $\varphi = 0.4$ , corresponds to the one located between the cup wall and the flange (i.e., Point 3), and it is followed by the region between the bottom and the cup wall where the highest  $\varphi$  value was 0.2.

After an experimental validation of the cooling curves simulated in the blank transfer phase, it was possible to analyze numerically the interaction between the plastic strain and temperature. For this purpose, the thermal and mechanical properties of the materials involved in the process that were calculated with the JMatPro<sup>®</sup> software, i.e., blank and tool steels, were considered. Thus, it was feasible to determine that the most critical forming region (i.e., Point 2) reached also the highest cooling rates. This is clearly indicated in the time–temperature sequences (red lines) of Figures 13 and 15. This is originated because it is also in this region where the highest contact pressures are developed, reaching values between 90 and 135 MPa (see Figure 14). In contrast, in the region where the highest plastic deformation develops (i.e., the point 3 region), the quenching does not become as drastic, since the contact pressures throughout this region are marginal (see Figure 14). In turn, these differences generate significant temperature gradients that could have a significant impact on alloys sensitive to these changes, or more explicitly, on the kinetics of precipitate formation during cooling. In this case, the most sensitive alloy of all those investigated is by far the X46Cr13 alloy.

Alloys X12Cr13 and X30Cr13 were not so sensitive to these temperature gradients, which were reflected in the resulting hardness values that remained generally homogeneous regardless of the initial forming temperature and workpiece region. In contrast, alloy X46Cr13 developed hardness values that were strongly dependent on the initial forming temperature and to a lesser extent on the workpiece region, as evidenced in Figure 10g–i.

The magnitude of the initial forming temperature sensitivity to time intervals was graphically detailed in the temperature–time sequences in Figure 16 for the X46Cr13 alloy. The temperature gradients in the workpiece at the end of the forming process varied significantly depending on the region and duration of the time interval. Temperatures at the end of the forming step varied between 750 and 600 °C, i.e.,  $\Delta T = 150$  °C. Accordingly, this is probably related to the resulting hardness as well as the hot drawability behavior. Nevertheless, it will be necessary to characterize the microstructure of the material to find a correlation in future work.

## 5. Conclusions

In this work, the hot deep drawability of the MSS alloys X12Cr13, X30Cr13, and X46Cr13 was experimentally evaluated. The maximum drawing depth was used for this purpose. Independently of the process parameters conditions, these alloy grades show a remarkable hot drawability. Nevertheless, due to chemical composition, the hot drawability performance and resulting hardness values are sensible to a variation of these parameters. The optimum parameters for each of the investigated MSS alloys are summarized in Table 5.

**Table 5.** Optimum deep drawing parameters for the investigated MSS alloys. This summary considered only the results with a  $\beta = 1.7$  (Blank  $\varnothing = 170$  mm), which showed the best results.

Alloy	Maximum Depth Drawability (up to 40 mm)				Quenchability	
	$T_{\gamma}$ (°C)/ $t_{\text{dwell}}$ (s)	Flange Gap (mm)	Initial Forming Temp. (°C)	$T_{\gamma}$ (°C)/ $t_{\text{dwell}}$ (s)	Initial Forming Temp. (°C)	Max. HV calc./Measured
X12Cr13	1150/300	2.5, 3.5 *	700 *, 800 *, 900	1150/300	700–900	451/480
X30Cr13	1150/300	2.5, 3.5	700, 800 *, 900 *	1150/300	800–900	578/657
X46Cr13	1150/300	2.5, 3.5	700, 800	1150/300	700–800	762/760

\* It was not evaluated experimentally but the results show a strong proclivity.

The plastic strain  $\varphi$  was determined by FE simulations. The highest level of  $\varphi$  was 0.4 and corresponds to that of the workpiece region located between the cup wall and the flange. The second region with the highest  $\varphi$  corresponds to the region between the bottom and the cup wall with a value of 0.2. The sensitivity of the initial forming temperature to the interval time during the blank transfer from the furnace to the tool was also determined. The 46Cr13 alloy was the most sensitive to this parameter, whereas the X12Cr13 and X30Cr13 alloys were more stable. The time intervals generated significant temperature gradients before the forming process that were extrapolated to the final temperature of the workpiece after forming. The final temperatures immediately after the forming process varied from 600 to 750 °C (i.e.,  $\Delta T = 150$  °C) depending on the region of the workpiece.

**Author Contributions:** Conceptualization, P.B., P.L., T.G. and E.M.-G.; experimental trials, P.B. and E.M.-G.; JMatPro® Software calculations, P.L. and T.G.; formal analysis E.M.-G., P.B. and V.K.; resources, V.K. and T.L.; supervision, V.K., T.G. and T.L.; funding acquisition, E.M.-G., P.L., V.K., and T.L. All authors have read and agreed to the published version of the manuscript.

**Funding:** Funded by the Deutsche Forschungsgemeinschaft (DFG, German Research Foundation)—Project number 334485458. The publication of this article was funded by Chemnitz University of Technology.

**Acknowledgments:** The authors gratefully acknowledge the support of the DFG.

**Conflicts of Interest:** The authors declare no conflict of interest.

## References

- McGuire, M. Chapter 9 Martensitic stainless steels. In *Stainless Steels for Design Engineers*, 1st ed.; ASM International: Materials Park, OH, USA, 2008; pp. 133–135.
- Gümpel, P. *Rostfreie Stähle—Grundwissen, Konstruktion und Verarbeitungshinweise*, Bd. 493; expert Verlag: Renningen-Malmsheim, Germany, 1996.

3. Karbasian, H.; Tekkaya, A.E. A review on hot stamping. *J. Mater. Process. Technol.* **2010**, *210*, 2103–2118. [[CrossRef](#)]
4. Meza-García, E.; Rautenstrauch, A.; Kräusel, V.; Landgrebe, D. Tailoring of mechanical properties of a side sill part made of martensitic stainless steel by press hardening. In *AIP Conference Proceedings, Proceedings of the 19th International ESAFORM Conference on Material Forming, Nantes, France, 27 April 2016*; Chinesta, F., Cueto, E., Abisset-Chavanne, E., Eds.; AIP Publishing: Melville, NY, USA, 2016; Volume 1769, pp. 1300015-1–1300015-5. [[CrossRef](#)]
5. Meza-García, E.; Rautenstrauch, A.; Kräusel, V.; Landgrebe, D. Press hardening of a martensitic stainless steel sheet alloy for manufacturing a side sill demonstrator with tailored properties. In *Proceedings of the 5th International Conference on Hot Sheet Metal Forming of High Performance Steel CHS2, Toronto, ON, Canada, 31 May–3 June 2015*; Steinhoff, K., Oldenburg, M., Prakash, B., Eds.; Publisher: Auerbach, Germany, 2015; pp. 765–773.
6. Mehner, T.; Landgraf, P.; Haack, E.; Scharf, I.; Grund, T.; Lampke, T. Pitting corrosion behavior of a laser hardened, high-alloyed steel. In *IOP Conference Series: Materials Science and Engineering, Proceedings of the 21st Chemnitz Seminar on Materials Engineering, Chemnitz, Germany, 6–7 March 2019*; IOP Publishing: Bristol, UK, 2019; Volume 480, p. 012018.
7. Momeni, A.; Dehghani, K. Characterization of hot deformation behavior of 410 martensitic stainless steel using constitutive equations and processing maps. *Mater. Sci. Eng. A* **2010**, *527*, 5467–5473. [[CrossRef](#)]
8. Chen, F.; Ren, F.; Chen, J.; Cui, Z.; Ou, H. Microstructural modeling and numerical simulation of multi-physical fields for martensitic stainless steel during hot forging process of turbine blade. *Int. J. Adv. Manuf. Technol.* **2016**, *82*, 85–98. [[CrossRef](#)]
9. Garcia, C.; Alvarez, L.F. Optimization of the properties obtained by quenching in martensitic stainless steels X30-40Cr13 and X40-60CrMoV14. *J. Mater. Sci.* **1993**, *28*, 1264–1268. [[CrossRef](#)]
10. Alvarez, L.F.; Garcia, C.; Lopez, V. Continuous cooling transformation in martensitic stainless steel. *ISIJ Int.* **1994**, *34*, 516–521. [[CrossRef](#)]
11. Saunders, N.; Guo, Z.; Li, X.; Miodownik, A.P.; Schillé, J.-P. Using JMatPro to model materials properties and behavior. *JOM* **2003**, *55*, 60–65. [[CrossRef](#)]
12. Landgrebe, D.; Rautenstrauch, A.; Kunke, A.; Polster, S.; Kriechenbauer, S.; Mauermann, R. The effect of cushion-ram pulsation on hot stamping. In *AIP Conference Proceedings, Proceedings of the 19th International ESAFORM Conference on Material Forming, Nantes, France, 27 April 2016*; Chinesta, F., Cueto, E., Abisset-Chavanne, E., Eds.; AIP Publishing: Melville, NY, USA, 2016; Volume 1769, pp. 070014-1–070014-6. [[CrossRef](#)]
13. Kusumi, K.; Nomura, N.; Yamamoto, S.; Nakata, M.; Abe, M.; Suehiro, M. Improvement of cylindrical deep drawability in hot stamping. *Procedia Eng.* **2014**, *81*, 1719–1724. [[CrossRef](#)]
14. Langrebe, D.; Kräusel, V.; Rautenstrauch, A.; Meza-García, E. Erweitertes Anwendungspotenzial von martensitischen nichtrostenden Stählen sowie von aushärtbaren Aluminiumlegierungen durch den thermomechanischen Blechumformprozess. In *Proceedings of the “23. Sächsische Fachtagung Umformtechnik”, Dresden, Germany, 7–8 December 2016*; pp. 52–61.

**Publisher’s Note:** MDPI stays neutral with regard to jurisdictional claims in published maps and institutional affiliations.



© 2020 by the authors. Licensee MDPI, Basel, Switzerland. This article is an open access article distributed under the terms and conditions of the Creative Commons Attribution (CC BY) license (<http://creativecommons.org/licenses/by/4.0/>).